Image Analysis for Assessing Molecular Activity Changes in Time-Dependent Geometries

Kostas Marias*, *Member, IEEE*, Jorge Ripoll, Heiko Meyer, Vasilis Ntziachristos, and Stelios Orphanoudakis, *Senior Member, IEEE*

***Abstract*—*In vivo* fluorescence molecular imaging and tomography has facilitated monitoring of genomics and proteomics over time and on the same animal. A highly important issue, however, has been the robust registration of animals imaged at different time points to obtain accurate description of activity and location. This paper presents a method for aligning temporal data of small animals based on surface anatomical features and improving the accuracy of monitoring fluorophore distribution. The method can account for differences in the positioning and compression of small animals and can be extended to three-dimensional as well as to other imaging modalities.**

***Index Terms*—Image registration, image sequence analysis, optical image processing.**

I. Introduction

IMAGE analysis has played an important role in the development of medical imaging, especially since it allowed the user to interact with the image, enhance its content, and extract valuable, quantitative information.

Molecular imaging is an emerging modality that is poised to have great impact in healthcare by providing more accurate and sensitive diagnosis and significantly improving treatment practices by early and highly specific visualization of drug activity [1]. Molecular imaging of small animals bears great importance in this new field as it is vastly used to: 1) evaluate new reporter technologies and imaging methods; 2) obtain new insights in *in vivo* processes and improve basic research; and 3) accelerate drug discovery in laboratory settings [2]. This new set of technologies comes with requirements for novel image analysis tools that can improve the accuracy of visualization and the information retrieved from planar images or tomographic reconstructions. This is particularly true in optical molecular imaging and tomography of whole animals, where the relative low resolution (∼0.5–1 mm [3]) and the absence of three-dimensional (3-D) anatomical information directs the development of novel approaches for image registration.

In this paper, we present a framework for correcting time-dependent geometries in two-dimensional (2-D) molecular optical imaging studies. A shorter account of our work with preliminary results in this area has been recently presented [4]. Our work also contributes in assessing the value of the proposed alignment technique in small animal imaging within an optical planar imaging setup, but can be extended to other modalities. Similar approaches may also de developed to analyze 3-D data. Previous experience on medical image registration (see [5]–[8] for selected publications in the field) is valuable for the design of the numerical methods for optical image alignment. However, although a plethora of both research and commercial tools is available, it has been proven in practice that it is not feasible to develop a generic, all-purpose tool for aligning any temporal image data; instead, experimentation is needed to assess the value of each method in a particular application. Based on previous work on mammogram registration [9], we propose here a method for aligning the boundary of small animals (mice) in successive sessions. Since optical methods do not provide internal landmarks, temporal image alignment (also known as image registration) is not perfect, and it is therefore important to assess the value of the method using data where the ground truth is known a priori.

The rationale for this work emanates from the use of optical imaging and tomography in tissues to detect and quantify molecular fluorescent probes over time on the same subject. This is in contrast to traditional studies that performed molecular analyses *in vitro* after sacrificing different animals at different time points. These capabilities gave rise to great advances in the use of light to probe molecular function, mainly due to the large number of specific fluorescent probes and reporter technologies (see [2] for a review on the subject). To date, two main techniques have been used for macroscopic imaging of fluorescence from animals. The first, termed fluorescence reflectance imaging (FRI) [10], [11] or fluorescence planar imaging, relies on photographic methods that record the surface distribution of fluorescence emitted from the animal. Similar practices are followed for bioluminescence imaging as well. The second and more recent technology, termed fluorescence-mediated molecular tomography or simply fluorescence molecular tomography (FMT) [12], produces 3-D spatial maps of fluorophore concentration using appropriate photon propagation forward models

Manuscript received July 15, 2004; revised March 29, 2005. The work of J. Ripoll and H. Meyer was supported by the European Union under Integrated Project "Molecular Imaging" LSHG-CT-2003-503259. The work of V. Ntziachristos was supported by the National Institutes of Health (NIH) under Grant ROI EB000750-1 and Grant R33 CA 91807. The Associate Editor responsible for coordinating the review of this paper and recommending its publication was G. Wang. *Asterisk indicates corresponding author.*

*K. Marias was with Medical Vision Laboratory, Department of Engineering Science, Oxford University, Oxford OX1 3PJ, U.K. He is now with the ICS-FORTH, GR 711 10 Heraklion, Greece (e-mail: kmarias@ics.forth.gr).

J. Ripoll and H. Meyer are with the Institute of Electronic Structure and Laser, Foundation for Research and Technology-Hellas, GR 711 10 Heraklion, Greece (e-mail: jripoll@iesl.forth.gr; heimeyer@iesl.forth.gr).

V. Ntziachristos is with the Center for Molecular Imaging Research, Massachusetts General Hospital, Harvard Medical School, Charlestown, MA 02129 USA (e-mail: vasilis@helix.mgh.harvard.edu).

S. Orphanoudakis, deceased, was with the Foundation for Research and Technology-Hellas, GR 711 10 Heraklion, Greece, and the Department of Computer Science, University of Crete, Heraklion, Greece.

Digital Object Identifier 10.1109/TMI.2005.848612

IEEE Proof

0278-0062/$20.00 © 2005 IEEE

and inversion techniques. Lately, FMT systems developed use similar geometry to that traditionally used for FRI and are capable of obtaining both reflectance and tomography data [3]. The tomographic approach in these systems resembles that of X-ray tomosynthesis, whereas limited angle projections are obtained and reconstructed for obtaining depth information. It is worth mentioning that, in typical 2-D planar-imaging studies, the bioluminescence (or fluorescence) image is usually superimposed over a white light image of the mouse in order to estimate the location of interest.

Optical imaging methods are noninvasive, thus opening the possibility of studying disease development, gene expression, cell trafficking, or agent/drug bio-distribution over a period of time on the same subject. However, when performing such experiments under different anaesthesia sessions—for example, over different days—it is difficult to ensure that the subject is placed in the exact same position, significantly complicating signal registration and quantification studies. These issues become more important in FMT studies that further resolve depth as well. To overcome such issues, we present a method that can account for geometrical distortions and compression differences, transforming the images measured at different stages so that they can be quantitatively compared. The proposed method has the potential to be useful in a large variety of applications that deal with lesion growth studies and/or migration, such as cell trafficking, tumor evaluations, and agent/drug biodistribution assessment.

The rest of this paper is structured as follows. In Section II, we describe the experimental setup and the methods for image alignment, while in Section III, we present the results, before concluding with a discussion in Section IV.

II. Experimental Setup and Methods

A. Experimental Setup

Fig. 1 is a schematic of the optical imaging setup used in this paper, where the subject is placed under constant white-light illumination and the reflected intensity is imaged on a charge-coupled device camera focused on the subject. This setup mimics those measuring planar fluorescence or bioluminesence images, and is equivalent to the imaging geometry used in [11] for fluorescence molecular tomography studies. The subject is held in position by using two plates controlling the distance between them, applying a slight compression to reduce movement.

B. Defining the Transformation Requirements

The development of image registration tools for optical data aims to provide the experimental platform with added functionality in handling time-dependent geometries. As in many cases in medical imaging, it is important to be able to account for motion in small animal imaging and crucial to improve the accuracy of monitoring fluorophore distribution.

The geometry of the problem is in general nonrigid, since the small animal can be slightly compressed in glass plates during the experiments. Even if great care is taken in positioning the animal, it is almost certain that differences in geometry will exist between successive sessions, especially if the animal is repositioned after a certain time interval. Nonrigid transformation is induced from either different positioning (e.g., twist) or from slight compression (e.g., in order to immobilize the animal).

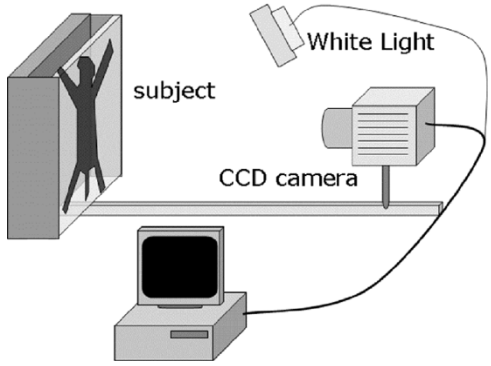


Fig. 1. Schematic view of the imaging system.

After experimenting with 2-D planar images, we have concluded that intensity-based alignment techniques such as optical flow or maximization of mutual information may not guarantee optimal results since the temporal displacement of the mouse in the image, as well as possible changes in compression, may be significant, leading to nonrigid motion. For this reason, we used a variation of a method that has been applied to temporal mammogram registration, based on thin-plate spline interpolation [9]. The analogy of this problem to the mammogram registration one is quite obvious, as in both cases the image appearance of an object is distorted over time due to changes in positioning and/or compression. The proposed method is described in the following sections and is composed of two basic steps: 1) invariant detection of the boundary of the small animal and 2) application of an interpolation technique to calculate the transformation.

C. Invariant Detection of Boundary Landmarks

In the cases when it is not possible to define robust internal landmarks such as the one at hand, the boundary of the subject is a very useful feature since it provides information about the difference in positioning/compression of the specimen between sessions. Moreover, since the shape of the mouse does not change significantly, landmarks can be defined in each pair of temporal images. This is done by using similar concepts with the work described in [9]. First, the region of interest (small animal) is isolated from the background using a generic image segmentation technique (e.g., watershed, or k-means clustering). Then, we use mathematical morphology (subtract a dilated version of the segmented image from the original) to obtain an eight-connected outline. Using triplets of sampled outline points, we then fit a parametric spline $\{x(s), y(s)\}$ and calculate the curvature at each point according to (1)

$$k(s) = \frac{x_{ss} \cdot y_s - x_s \cdot y_{ss}}{x_s^2 + y_s^2} \tag{1}$$

where x_s, x_{ss} and y_s, y_{ss} are the first and second derivatives of $x(s)$, $y(s)$ with respect to s (the curvilinear parameter s describes the outline). If the segmentation result is jagged, then by increasing the sampling rate, the boundary can be smoothed.

IEEE Proof

This way, the presented method can also be implemented in a multiscale fashion (e.g., by computing a curvature scalogram as in [9]) to improve robustness. In order to do this, the sampling rate can be gradually increased, and each time landmarks are computed as curvature maxima. By plotting all landmarks defined at each scale, the "persistent" ones can be detected on the basis of propagation through scale-space.

At a given scale, landmarks are detected as shown in Fig. 2 by analyzing the curvature profile of the sampled boundary. The top right image shows the mouse in its original position, while the bottom right one is the result of applying a random, realistic nonrigid transformation. By comparing the curvature profiles (shown on the left), we can see that the maximum curvature points along the boundaries are transformation invariant. These points are detected by thresholding the curvature profiles at the 25% of maximum curvature (to eliminate small curvature points and noise), then followed by a clustering technique (in our experiments we use fuzzy clustering) to group high-curvature points.

In fact, clustering is used in order to group together the neighboring, high-curvature points of each curvature maximum so as to increase detection robustness. Such maxima correspond to anatomical entities (e.g., upper right limb). The points displayed in Fig. 2 (right) are the maximum curvature points of each cluster. It is also noticeable that the curvature profiles are consistent and the small shift is due to the random selection of the starting point along the outline. In this paper, we only considered the "positive" curvature profile (moving along the boundary in a clockwise direction, the tangent vector at each positive curvature segment points outwards from the object). By considering the "negative" value curvature profile, additional maximum curvature points could be detected.

We have experimented with a large variety of possible transformations and have concluded that, in almost all realistic transformation scenarios, the detection of such points is consistent. Limitations of the method are discussed in the concluding section of this paper. These points could be the basis of a generic, semiautomatic algorithm for landmark definition. It is important to mention that the robust detection of landmarks is crucial for any feature-based image alignment method. For this reason, in a real application scenario, the user must be able to interact and, if necessary, correct the location of the landmarks. Once point correspondences are defined, each pair of images is registered as is explained in the next section.

D. Transform Estimation Using Interpolation

The basic method used for interpolation is based on thin-plate splines (see [13] for an analytical description). Based on the calculated landmarks, a smooth interpolating function $\mathbf{t}(x, y)$ is calculated for the vertical and the horizontal direction. Using this function, the image is deformed in such a way that the bending energy is minimized, while matching the landmarks. The bending energy is given by (2)

$$J_2^2(\mathrm{t}) = \iint \left[\left(\frac{\partial^2 \mathrm{t}}{\partial x^2} \right)^2 + 2 \cdot \left(\frac{\partial^2 \mathrm{t}}{\partial x \partial y} \right)^2 + \left(\frac{\partial^2 \mathrm{t}}{\partial y^2} \right)^2 \right] dxdy. \tag{2}$$

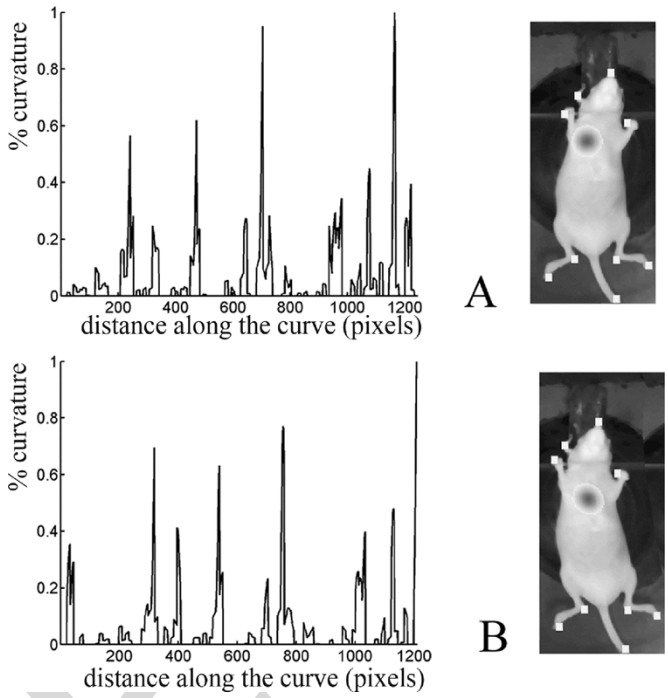


Fig. 2. Transformation-invariant landmark detection in two different positioning scenarios (A, B) based on the curvature profiles (shown on the left).

This method is efficient at recovering local deformations, but special care is needed in the selection of the landmarks since it does not account for possible inaccuracies in their localization.

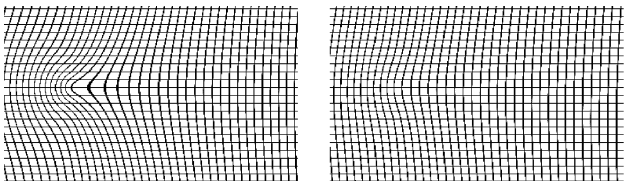
When there is noise in the specified values, or a large number of landmarks is detected with a global method (e.g., filters), one may wish to relax the exact interpolation requirement by means of regularization. Rohr *et al.* [14] suggested the weakening of the interpolation condition in such a way that the resulting transformation is a compromise between smoothness and data adaptation. The new functional $J_\lambda(\mathbf{t})$ to be minimized is a function of λ, a regularization parameter that controls the balance between the smoothness and the approximation of the transformation

$$J_\lambda(\mathrm{t}) = \sum_{i=1}^{n} \frac{|\mathrm{q_i} - \mathrm{p_i}|^2}{\sigma_i^2} + \lambda \cdot J_2^2(\mathrm{t}) \tag{3}$$

where $\mathbf{q}_i$ and $\mathbf{p}_i$ are the landmark pairs, σ_i is the individual weight for each landmark pair i, $J_2(\mathbf{t})$ is the bending energy of the transformation $\mathbf{t}$, and λ is a parameter that controls the tradeoff between the smoothness of the transformation and adaptation to the local transformations induced by the data. λ may vary between zero (very good approximation of the landmarks) to ∞ (very smooth transformation with very little adaptation to local deformations). This is illustrated in Fig. 3, where λ increases from zero to 10^4, resulting in a smooth transformation that however does not conform to the landmark coordinates. It is obvious that λ should be increased only if uncertainly is present (i.e., to regularize a flow); otherwise (if landmarks are trusted), accuracy may be compromised.

Landmark localization can be based on the curvature analysis described in Section II-C. In order to maintain the anatomical information conveyed, all landmarks are equally weighted, since

IEEE Proof



(a) (b)

Fig. 3. Increasing λ from (a) zero to (b) 10^4 leads to a smooth transformation that does not conform to the landmarks. The landmarks used are the same in both cases.

the presented curvature matching method is a deterministic approach. In addition, λ is kept to one in order to conform to the transformation induced by the computed landmarks. It is sensible to increase λ when differences in landmark localization uncertainties are introduced or a large set of landmarks is computed, e.g., by using a filter.

To improve accuracy, it is also possible to sample between pairs of detected transformation-invariant points. Increasing the number of landmarks may induce a small improvement in alignment accuracy, however, at the cost of additional computational time. In this paper, this is not investigated since the compromise between benefit and increased computational time will depend on the specific application setup.

After the transformation is computed, the template image can be aligned to the target one. When applying the mapping function $\mathbf{t}(x, y)$ [calculated by minimizing (2) or (3)], it is often the case to fall outside the orthogonal pixel grid (i.e., the transformed coordinates are not integers). In these cases, a pixel interpolation method is needed. In this paper, bilinear interpolation has been used; however, it has been recently shown that the choice of the interpolation method can affect the intensity profile of the image [15].

Validation results are presented in the next section.

III. Results

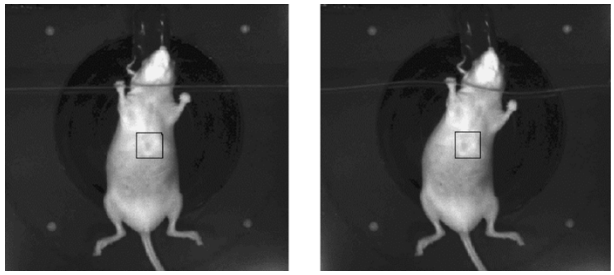
A. Design and Description of the Experiments

An important contribution of a temporal image alignment method in molecular imaging could be to improve the accuracy of cell tracking. In order to assess the value of image alignment, it is important to design experiments where the ground truth is known a priori. In a real scenario, the exact location of the targeted cells is unknown, and for this reason we designed both synthetic and real experiments.

In Section III-B, a complex nonrigid transformation (twirl) is applied to a mouse image and the alignment process is explained in detail. The result is also assessed quantitatively.

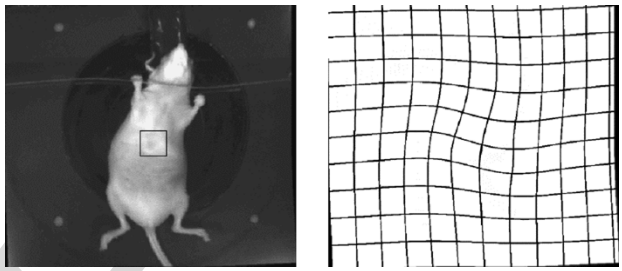
The second validation experiment (Section III-C) is on synthetic data, produced numerically, by moving the location of the fluorophore distribution and then randomly and nonlinearly transforming the image. This is an important experiment for cell tracking since it clearly reveals the potential but also the limitations of the suggested method.

Lastly, the final experiment (Section III-D) is done using fiducial markers drawn in the abdomen of an anaesthetized nude mouse. The goal here is to evaluate the usefulness of the method in tracking specific anatomical positions over time. Special care was taken to minimize the errors that could be introduced due to skin stretching. In essence, this experiment mimics the fluorophore tracking scenario by introducing invariant markers, inducing a positioning-related nonrigid transform and measuring the error before and after alignment.



(a) (b)

Fig. 4. (a) Template and (b) target image. An AOI is highlighted.



(a) (b)

Fig. 5. (a) Transformed template to target with an AOI highlighted and (b) the deformed grid.

Finally, it should be noted that in the following experiments there was no rigid displacement (e.g., translation) between the image sequences (i.e., before alignment image pairs were as rigidly aligned as possible). This was done so as to assess the added value of the method, assuming that in a given setup care is taken to ensure that the imaging geometry is as consistent as possible, eliminating rigid differences between sessions.

B. Inducing a Complex Nonrigid Transformation

The design of the first experiment aims to test that the computation of the suggested landmarks is appropriate for estimating nonrigid deformations in time dependent geometries. This way, we assess the value of techniques that have been previously used for recovering soft tissue deformations (e.g., in breast imaging), in small animal imaging. In addition, this experiment investigates whether the internal region correspondence is improved.

Fig. 4 shows the template image (on the left). The target image (on the right) is produced by applying an unknown, complex nonlinear transformation (twirl) while no extra-noise is added since the landmark detection method is geometrical and therefore photometrically invariant. In both images a specific area of interested is highlighted (enclosed by a square) in order to also assess the internal registration error. The method presented in Section II is applied to both images in order to compute the boundary landmarks. After applying the computed transformation function, the template image is registered to the target, as shown in Fig. 5.

IEEE Proof

Mutual information (see [16] for a description of such techniques) can be used to evaluate the similarity of the segmented template and target image before and after alignment. In this particular experiment, it was increased from 0.52 to 0.73 (40%).

In molecular imaging, it is very important to accurately follow the evolution of a particular region in successive sessions. This process can be prone to error, and image registration might be useful. Fig. 6(a) illustrates that the error (difference) image before registration exhibits strong misalignments that are significantly reduced after alignment, as shown in Fig. 6(b). It should be noted that both error images were histogram equalized so that all the differences could be clearly visible and that the same area of interest (AOI) as before is highlighted. Fig. 6(c) is the magnification of the square enclosing the area of interest from the target (the ground truth AOI). Fig. 6(d) is the magnification of the same region in the postalignment error image [Fig. 6(b)]. It is clear that the AOI is well aligned as the edge definition is consistent to the "ground truth AOI" [Fig. 6(c)]. In contrast, the two artifacts in Fig. 6(e), suggest that nonrigid image alignment is a potentially crucial step in quantitatively assessing AOIs over time (e.g., a cancer).

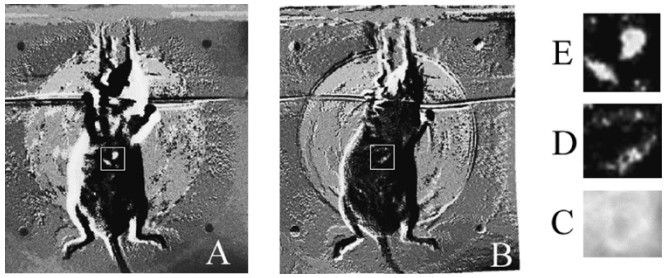


Fig. 6. (A) Error image before alignment, (B) error image after alignment, (C) "ground truth" area of interest in the target image, (D) same AOI in the error image (B) after alignment, and (E) same AOI in the error image (A). Without alignment the assessment of the region of interest over time is prone to error artifacts [as is shown in (E)].

C. Synthetic Fluorophore Data Experiment

Since in a real scenario the exact location of the targeted cells is very hard (if possible) to define, we designed a synthetic fluorophore tracking experiment. Synthetic, fluorescence imaging data of molecular activity inside a mouse are produced numerically by moving the location of the fluorophore distribution and then randomly and nonlinearly transforming each image (instance of motion). This way, we simulate time-dependent positioning and exerted compression on the subject (mouse), that result in both rigid and nonrigid changes in the shape of the imaged subject. Further, temporal inhomogeneities present in a realistic situation (e.g., lighting, noise, etc.) are not simulated because they do not affect the geometrical definition of landmarks since it only depends on the curvature transitions, which in turn correspond to the anatomy structure of the animal (in Section III-C such differences do exist).

In order to simulate the fluorescence map emitted from the subject, we have made use of the diffusion approximation, modeling the mouse as an infinite slab. This approach has been used, for example, in FMT studies yielding accurate results (see [3]). Since we are interested in studying the positional error introduced when considering time-dependent situations, we have considered the case of a constant distribution of fluorophores that moves along the same XY plane (i.e., parallel to the detection plane) at a distance of 0.75 cm from the surface.

Fig. 7 shows the ground truth data used for a validation experiment. Using only one image of the mouse with the fluorophores superimposed, we simulate the propagation of a constant distribution of fluorophores in seven different instances. Notice that in Fig. 7, the geometry of the mouse is unchanged and each location of the fluorophores is used as the ground truth. Then, a random transformation is applied to each image (2–7) in order to simulate the random changes in positioning and compression. This way, we want to validate the accuracy of our method in recovering these random transformations and locating the site

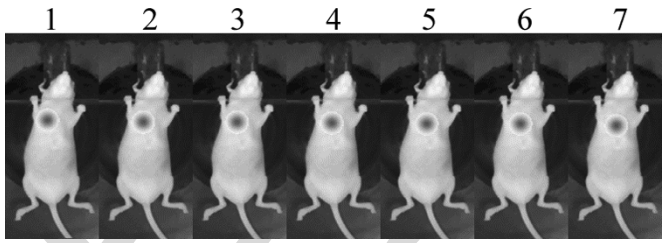


Fig. 7. The validation data consist of seven identical images of the mouse except for the distribution of fluorophores that is simulated to propagate inside the mouse within a plane parallel to the detection plane at 0.75 cm from the surface.

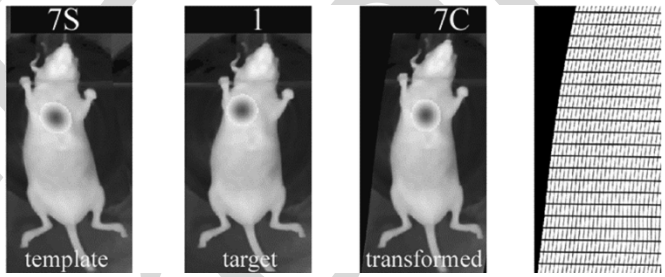


Fig. 8. The simulated image 7S is aligned with image 1 of the "ground truth" dataset (i.e., image 1 in Fig. 7), resulting in the "corrected" image 7C. The last image on the right is the computed transformation grid.

of the fluorophores (center of distribution) in each simulation (2–7). This is further explained in Fig. 8, where a random transformation is applied to the seventh image of Fig. 7. The simulated image (7S) is then aligned with image 1 of Fig. 7, resulting in the "corrected" image 7C.

This process is repeated for images 2–6. In order to validate the accuracy of the method, the location of the center of mass of the fluorophore distribution of the simulated and corrected data-set is compared to the "ground truth" values. Fig. 9 shows the distance of all fluorophore center points from the "ground truth" origin point (fluorophore position "1" in Fig. 7). Specifically, we plot the "ground truth" trajectory of the fluorophore center and compare it to the fluorophore trajectories of the original simulated and corrected data-sets. The graph clearly indicates that the proposed method significantly recovers most nonrigid distortions caused by differences in positioning of the mouse.

IEEE Proof

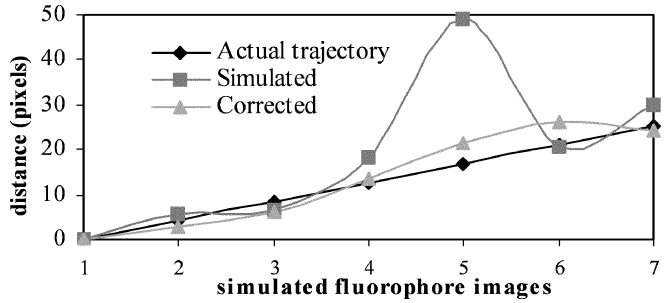


Fig. 9. The actual trajectory of the fluorophores compared to the trajectories calculated from the simulated and corrected datasets (pixel size in this configuration is 0.037 cm).

D. Introducing Fiducial Markers for Validation

Six markers at a distance of 0.5 cm from each other were drawn in the abdomen of an anaesthetized mouse [Fig. 10(a)]. By carefully changing the geometry of the mouse, we introduced a significant nonrigid displacement [Fig. 10(b)]. The locations of the six markers were then used to assess the accuracy improvement in the correspondence of the six points.

The working assumption is that the markers must be at exactly the same location in both images (i.e., the error distances should be zero). The marker that is closest to the tail is numbered as "1" and the one closest to the head as "6."

By using $n = 8$ boundary landmarks (as in Section II-C except for the ear that is not visible), and then solving the minimizing problem [(2), (3)], each point of Fig. 10(b) is mapped to A, according to the vector-valued function $\mathbf{t}(x, y) = [f_x(x, y), f_y(x, y)]$, where

$$f_k(x,y) = \alpha_{1k} + \alpha_{2k}\cdot x + \alpha_{3k}\cdot y + \sum_{i=1}^{n} w_{ik}\cdot U\left(|(x_i, y_i) - (x, y)|\right) \tag{4}$$

where $k = \{x, y\}$, $[\alpha_1, \alpha_2, \alpha_3]$ are the rigid coefficients, w_i the nonrigid coefficients (both are calculated from the solution of the linear systems described in [13], [14]), (x_i, y_i) are the boundary landmarks, and $U(r) = r^2\ log\ r^2$. Since the landmarks are anatomical, the value of λ is set to one in order to avoid error amplification due to smoothing (as illustrated in Fig. 3). This way we transform the coordinates of each one of the six source-fiducials $\boldsymbol{P}_{\text{si}}$ (centers of spots in Fig. 10(b)) and calculate the error with respect to each target-fiducial $\boldsymbol{P}_{\text{ti}}$ point [in Fig. 10(a)] according to (5)

$$\boldsymbol{error} = \boldsymbol{P}_{\text{ti}} - \mathbf{t}(\boldsymbol{P}_{\text{si}}), \quad i = 1 - 6. \tag{5}$$

This way, the displacement error of the markers before and after alignment is assessed and the results are shown in Fig. 11. Before registration, fiducials 4–6 (close to the head) in Fig. 10(b) are nonlinearly displaced [errors are $\sim -180^\circ$ with respect to the "target" fiducial-markers location in Fig. 10(a)]. The rest of the fiducials (1–3) overlap in both Fig. 10(a) and (b). Using the calculated transformation $\mathbf{t}$, the mouse image B is warped to A (bilinear interpolation is used for transformations that fall outside the orthogonal grid). In Fig. 10(c), the transformed mouse is shown overlayed on the corresponding transformed grid. After registration, all fiducial-markers overlap (at least partially).

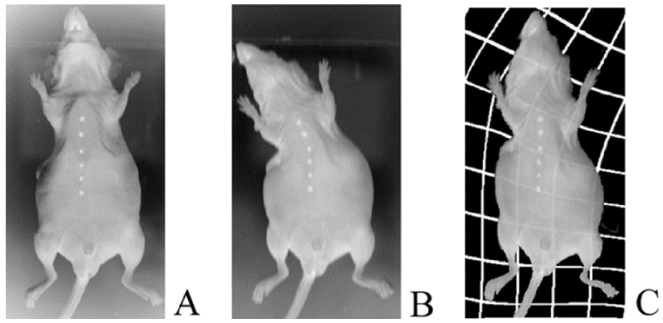


Fig. 10. (A) The anesthetized mouse with the six markers drawn on its abdomen. (B) Nonrigid displacement of the mouse while special care is taken so as not to alter the skin stretching. (C) The transformed mouse (B) aligned to the coordinates of (A) (pixel size corresponds to 0.17 mm). We here show the negative of the images in order to improve contrast.

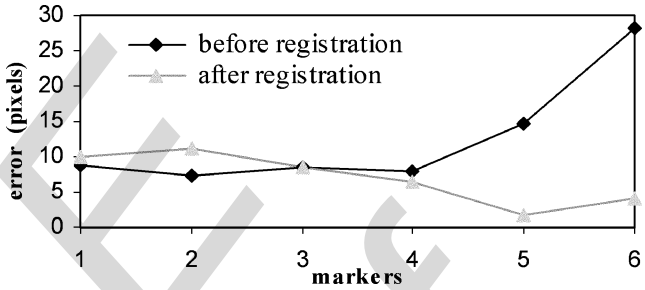


Fig. 11. The distance error in the fiducial markers location before and after alignment. There is an overall improvement, which is however significant only for the markers toward the head of the mouse where the deformation is larger (pixel size corresponds to 0.17 mm).

It is clear that the benefit from the application of the method strongly depends on the original displacement of the markers; the larger the displacement, the better the improvement in alignment accuracy. It is also worth mentioning that the error in localization of marker "2" is marginally larger in the registered images. However, this can be attributed to numerical errors (e.g., marker coordinates localization) since the error distance of markers "2" (from tail to head) in the unregistered image pair is less than 10 pixels (corresponding to 1.7 mm, which practically means that markers exhibit overlap). The assessment of alignment improvement with respect to the initial displacement is an important issue that needs further evaluation in controlled, ground truth experiments. However, we need to stress that it is difficult to set up such experiments. The results shown in Fig. 11 suggest that correspondence can be improved when tracking cells or lesions in time-dependent geometries.

IV. Discussion

A method for the alignment of 2-D optical imaging data was presented. The method is based on detecting invariant landmarks on the boundary of the imaged subject. The basic limitation of the method is that it assumes consistency in the anatomical and angle of view information present on both temporal images. However, this assumption does not limit the applicability of the method in practice; rather, special care is needed to position the subject in an anatomically consistent way (e.g., parallel to the working surface with all limbs extended). Similar to other imaging domains such as X-ray breast cancer imaging,

IEEE Proof

care must be taken to avoid twists that will change the angle of view with respect to the previous session. Lastly, it should be noted that there are intrinsic limitations in any landmark-based method, and if greater accuracy is needed (e.g., few millimeter accuracy requirements arising from high specificity and sensitivity needs), a new, holistic approach, exploiting also acquisition characteristics, could define a next research direction to the problem.

In our experiments, every effort was made to preserve both the anatomical information and the angle of view, as much as possible. In cases, however, where, e.g., one extremity is not present in the image of a subsequent session, a bad match can also be avoided on the basis of poor curvature similarity. It should be noted that in our studies compression is minimal, aiming only to keep the animal in place. Larger compressions can induce more complex internal tissue motions.

Both synthetic and real experiments were performed to recover the location and shape of a region of interest (Section III-B), the simulated fluorophore motion (Section III-C), and the marker's location (Section III-D). In all the experiments, the nature of the transformation was nonrigid and the unregistered images were rigidly aligned (i.e., there was no translation). The results indicate that temporal correspondence can be improved. Additionally, the larger the initial displacement of a region of interest, the better the improvement in marker localization. The results in Section III-D indicate that fiducial error can be reduced to less than 1.7 mm. However, it should be noted that by using landmarks far away from the region of interest, the accuracy of the deformation field inferred may be insufficient for applications requiring high accuracy in tracking internal regions. Nevertheless, correspondence of regions can become more consistent. The method can be easily implemented and used in a large variety of fluorescence reflectance imaging, bioluminescence imaging, and most positron emission tomography and single-photon emission computed tomography applications that need several imaging sessions, such as cell trafficking, tumor growth factor, and others, potentially improving the resolution and quantization.

ACKNOWLEDGMENT

K. Marias would like to acknowledge the endless support of S. Orphanoudakis who passed away during the review procedure of this paper.

REFERENCES

[1] R. Lamerichs, T. Schäffter, Y. Hämisch, and J. Powers, "Molecular imaging: the road to better healthcare," *Medica Mundi*, vol. 47, no. 1, 2003.

[2] R. Weissleder and V. Ntziachristos, "Shedding light onto live molecular targets," *Rev. Nat. Med.*, vol. 9, no. 1, pp. 123–128, 2003.

[3] E. E. Graves, J. Ripoll, R. Weissleder, and V. Ntziachristos, "A submillimeter resolution fluorescence molecular imaging system for small animal imaging," *Med. Phys.*, vol. 30, no. 5, 2003.

[4] K. Marias, J. Ripoll, V. Ntziachristos, and S. Orphanoudakis, "Non-rigid image transformation for assessing changes in fluorescence imaging data of molecular activity in time-dependent geometries," in *Proc. IEEE Int. Symp. Biomedical Imaging: Macro to Nano*, 2004, pp. 484–487.

[5] A. Guimond, A. Roche, N. Ayache, and J. Meunier, "Multimodal brain warping using the demons algorithm and adaptive intensity corrections," *IEEE Trans. Med. Imag.*, vol. 20, no. 1, pp. 58–69, Jan. 2001.

[6] T. McInerney and D. Terzopoulos, "Deformable models in medical image analysis: a survey," *Med. Image Anal.*, vol. 1, no. 2, pp. 91–108, 1996.

[7] G. P. Penney, J. Weese, J. A. Little, D. L. G. Hill, and D. J. Hawkes, "A comparison of similarity measures for use in 2-D-3-D medical image registration," *IEEE Trans. Med. Imag.*, vol. 17, no. 4, pp. 586–595, Aug. 1998.

[8] J. B. Antoine Maintz and M. A. Viergever, "A survey of medical image registration," *Med. Image Anal.*, vol. 2, no. 1, pp. 1–36, 1998.

[9] C. P. Behrenbruch, K. Marias, P. A. Armitage, M. Yam, N. Moore, R. E. English, P. J. Clarke, and M. Brady, "Fusion of contrast-enhanced breast MR and mammographic imaging data," *Med. Image Anal.*, vol. 7, no. 3, pp. 311–340, 2003.

[10] U. Mahmod, C. H. Tung, A. Bogdanov, and R. Weissleder, "Near-infrared optical imaging of protease activity for tumor detection," *Radiology*, vol. 213, pp. 866–870, 1999.

[11] C. H. Contag, D. Jenkins, P. R. Contag, and R. S. Negrin, "Use of reporter genes for optical measurements of neoplastic disease *in vivo*," *Neoplasia*, vol. 2, pp. 41–52, 2000.

[12] V. Ntziachristos, C. Tung, C. Bremer, and R. Weissleder, "Fluorescence-mediated tomography resolves protease activity *in vivo*," *Nat. Med.*, vol. 8, pp. 575–560, 2002.

[13] F. Bookstein, "Principal warps: Thin-plate splines and the decomposition of deformations," *IEEE Trans. Pattern Anal. Mach. Intell.*, vol. 11, no. 6, pp. 567–585, Jun. 1989.

[14] K. Rohr, H. S. Stiehl, R. Sprengel, T. M. Buzug, J. Weese, and M. H. Kuhn, "Landmark-based elastic registration using approximating thin-plate splines," *IEEE Trans. Med. Imag.*, vol. 20, no. 6, pp. 526–534, Jun. 2001.

[15] J. Tsao, "Interpolation artifacts in multimodality image registration based on maximization of mutual information," *IEEE Trans. Med. Imag.*, vol. 22, pp. 854–864, Jul. 2003.

[16] J. Pluim, J. Maintz, and M. Viergever, "Mutual information based registration of medical images: a survey," *IEEE Trans. Med. Imag.*, vol. 22, no. 8, pp. 986–1004, Aug. 2003.

IEEE PROOF